

# The Sun as an X-ray Star: III. Flares

F. Reale, G. Peres

*Dip. di Scienze Fisiche & Astronomiche – Sez. di Astronomia –  
Univ. di Palermo, Piazza del Parlamento 1, I-90134 Palermo, Italy;  
reale@astropa.unipa.it, peres@astropa.unipa.it*

S. Orlando

*Osservatorio Astronomico, Piazza del Parlamento 1, I-90134 Palermo, Italy;  
orlando@astropa.unipa.it*

## ABSTRACT

In previous works we have developed a method to convert solar X-ray data, collected with the Yohkoh/SXT, into templates of stellar coronal observations. Here we apply the method to several solar flares, for comparison with stellar X-ray flares. Eight flares, from weak (GOES class C5.8) to very intense ones (X9) are selected as representative of the flaring Sun. The emission measure distribution vs. temperature, EM(T), of the flaring regions is derived from Yohkoh/SXT observations in the rise, peak and decay of the flares. The EM(T) is rather peaked and centered around  $T \approx 10^7$  K for most of the time. Typically, it grows during the rise phase of the flare, and then it decreases and shifts toward lower temperatures during the decay, more slowly if there is sustained heating. The most intense flare we studied shows emission measure even at very high temperature ( $T \approx 10^8$  K). Time-resolved X-ray spectra both unfiltered and filtered through the instrumental responses of the non-solar instruments ASCA/SIS and ROSAT/PSPC are then derived. Synthesized ASCA/SIS and ROSAT/PSPC spectra are generally well fitted with single thermal components at temperatures close to that of the EM(T) maximum, albeit two thermal components are needed to fit some flare decays. ROSAT/PSPC spectra show that solar flares are in a two-orders of magnitude flux range ( $10^6 - 10^8$  erg cm<sup>-2</sup> s<sup>-1</sup>) and a narrow PSPC hardness ratio range, however higher than that of typical non-flaring solar-like stars.

*Subject headings:* Sun: activity, Sun: corona

## 1. Introduction

Because of its closeness, the Sun is the best-observed and the only spatially-resolved X-ray star. It is therefore natural to consider it as a template and a guide to analyze and interpret what we observe of the other stars.

In this perspective two previous works (Orlando et al. 2000, Peres et al. 2000a, hereafter Paper I and Paper II, respectively) illustrate a method to put solar X-ray data collected by the *Soft X-ray Telescope* on board Yohkoh into the same format and framework as stellar X-ray data. The method allows us to simulate accurately the observation of the Sun at stellar distances with a stellar instrument and to apply to the relevant data the same analysis as if they were real stellar data: we can compare homogeneously stellar to solar data and use the latter as a template for stellar observations.

Paper I focussed on the details of the treatment of Yohkoh data and Paper II outlined the method in its generality and showed some representative applications to observations in different phases of the solar cycle plus one flare case. The present work applies this analysis to several solar flares in the perspective to interpret stellar flares and some features of very active stellar coronae.

Coronal flares are transient, X-ray bright and localized events: they last from few minutes to several hours, they easily overcome the luminosity of the whole solar corona and they occur in relatively small regions, often in single coronal magnetic structures (loops). As such their occurrence and evolution is mostly independent of the structure and evolution of the rest of the corona. Since the phenomenology, duration and intensity can be very different from one flare to another it is difficult to take a single flare as representative. In this work we analyze the emission measure distribution vs. temperature and its evolution during some selected solar flares, representative of the wide range of possible events; as we did in Paper II we then use these EM(T)'s to synthesize relevant stellar-like spectra, which are then analyzed with standard analysis tools of stellar coronal physics.

Together with the general problem of the structure and heating of the solar corona, flares represent an unsolved puzzle of Solar Physics. Their early impulsive phase is so fast that the trigger mechanism remains elusive, in spite of the high quality of the data collected with many instruments, and in particular with the Yohkoh/SXT, optimized to observe flares. Apart from experimental limitations, intrinsic physical reasons make the diagnostics of the flare heating very difficult: the flare starts when a low density plasma is heated at more than  $10^7$  K; due to the low emission measure, initially the plasma is not easily observable while thermal conduction is so efficient that it smoothes out in a few seconds any trace of local thermal perturbation. The rise of the brightness in the soft X-ray band, where flares are

best-observed, does not follow the evolution of the heating (e.g. Reale & Peres 1995).

While analysing the rise phase is useful to investigate the mechanisms which originate the flares, the decay phase has been shown to be useful in other respects. It has long been known that the duration of the decay is linked to the size of the flaring region, because the thermal conduction cooling time depends on the length of the flaring loops. This has direct implications on stellar flares: from the observed light curve it has been possible to estimate the size of the unresolved stellar flaring loops. On the other hand it has also been shown that the estimates based on simple scalings from the conduction or radiation cooling times only can be largely incorrect: indeed, significant heating can be present (Jakimiec et al. 1992) and sustain the solar and stellar flare decays (Reale et al. 1997, Reale & Micela 1998, Schmitt and Favata 1999, Favata et al. 2000, Maggio et al. 2000) longer than expected, therefore leading to very coarse loop lengths overestimates. A useful tool to identify the presence of such a prolonged heating is the flare density-temperature diagram: the longer the heating decay (compared to the free cooling loop decay time, Serio et al. 1991), the smaller is the slope of the decay in this diagram (Sylwester et al. 1993). Knowing the decaying light curve and the path in the density-temperature diagram leads us to obtain reliable estimates of the flaring loop length and of the heating in the decay phase (Reale et al. 1997).

The analysis of stellar flares have been often based on loop models (e.g. Reale et al. 1988, van den Oord et al. 1988, van den Oord & Mewe 1989, Reale & Micela 1998). The present study, instead, uses solar flares really observed and spatially resolved by the Yohkoh/SXT as templates: we will apply here the method illustrated in Papers I and II to obtain the evolving EM(T) and stellar-like flare spectra as observed by non-solar instruments, in particular the *Solid-state Imaging Spectrometer* (SIS) on board the *Advanced Satellite for Cosmology and Astrophysics* (ASCA) and the *Position Sensitive Proportional Counter* (PSPC) on board the *Röntgen Satellit* (ROSAT), which have been among the most used X-ray observatories for the observation of stellar coronae.

It is interesting to apply the standard stellar spectra analysis to the resulting flare spectra and see analogies and differences from really observed stellar flares. The advantages of this approach are that: i) it is relatively model-independent (only spectral models have to be included); ii) it analyzes the whole flaring region including contributions from structures adjacent but outside the dominant (if any) loop, or, in the case of arcade flares, from many loops.

Spectra of several intense (and therefore yielding good count statistics) stellar flares collected by ROSAT (e.g. Preibisch et al. 1993, Ottman et al. 1996) and especially by ASCA (e.g. Gotthelf et al. 1994, Güdel et al. 1999, Osten et al. 2000, Hamaguchi et al. 2000, Tsuboi et al. 2000) have been analyzed in the recent past. In order to yield a count

statistics appropriate for a sound analysis, each spectrum is typically integrated on time intervals spanning significant fractions of the flare, therefore averaging on rapidly evolving plasma and emission conditions. In spite of this, spectrum models of isothermal plasma (1-T models) are generally able to describe each spectrum (subtracted by the quiescent "background" spectrum) with temperatures and emission measures following expected solar-like trends. The peak temperatures of analyzed stellar flares are quite higher, and their emission measures orders of magnitude higher ( $> 50MK$  and  $> 10^{54} \text{ cm}^{-3}$ , respectively), than typical solar ones. Deviations from the single temperature description have been also detected (Ottmann & Schmitt 1996, Favata et al. 2000). It is interesting in this context to investigate if there is correspondence with analogous spectra synthesized from solar flares which may then be used as templates to interpret stellar flare spectra.

A debated question about stellar flare spectra is the fact that many of them are better fit by allowing the metal abundance to vary in the fitting model. The spectra are acceptably fit with metal abundance increasing in the rising phase and then decreasing gradually in the decay (Ottman et al. 1996, Favata et al. 2000). The physical meaning of this result is still far from being settled. Wherever possible, it has also been shown that the abundance variations seem to change element by element (Osten et al. 2000, Güdel et al. 1999).

Although the problem of abundance variations in stellar coronae is intriguing, far from being settled and addressed by several investigations with XMM-Newton (*X-ray Multi-Mirror Mission*) and Chandra satellites (e.g. evidence for an inverse First Ionization Potential effect has been found on the star HR1099, Brinkman et al. 2001), the approach presented here does not allow to investigate it properly. What we can do is to explore the effect of allowing abundances to vary in fitting spectra originating from parent multi-thermal emission measure distributions.

In this study beyond the extrapolation of the solar flares to the stellar environment as isolated, self-standing and evolving events, we will also focus on their possible contribution to make up the emission of very active coronae. In this respect, evidence has been collected from multi-line XUV observations that the emission measure of some active stellar coronae has two peaks, one at a few  $10^6$  K and the other at  $\sim 10^7$  K and it has been proposed that the higher temperature peak is due to a continuous flaring activity (e.g. Güdel 1997, Drake et al. 2000). Paper II addressed, although limitedly, the evidence from extensive ROSAT observations that solar-like stars cover an extended region in the plane flux/hardness ratio (Schmitt 1997), while the Sun, as a whole, spans the low HR-low flux part of the same region. In this context it is worth investigating the region occupied by flares.

This work is structured as follows: in Section 2, we describe the solar data and our analysis for the derivation of the flare EM(T)'s and of the stellar-like spectra; Section 3

shows the results obtained for our sample of Yohkoh/SXT flares, the related stellar-like spectra, collected with ASCA/SIS and ROSAT/PSPC, and their analysis with standard stellar methods; in Section 4 we discuss our results and draw our conclusions.

## 2. The data analysis

### 2.1. The Yohkoh flare data

In order to study the EM(T) distribution of solar flares, we have selected a sample of flares well-observed for most of their duration by Yohkoh/SXT and covering a wide range of flare intensities and physical conditions. In particular we have selected eight flares ranging from relatively weak (class C5.8) to very intense flares (X9.0). The flares and their SXT observations are listed in Table 1, along with the date and time of the flare beginning as measured with the *Geosynchronous Operational Environmental Satellite* (GOES), the GOES class, the duration of the flare as in the GOES log file, and the start, maximum emission measure and end times of the SXT observations. The observations monitor large fractions of the rise, peak and decay of the thermal phase of the flares.

The analyzed data include the SXT data taken in flare mode, and, in particular, in the two filter passbands specific for flare mode observations, i.e. Be 119  $\mu\text{m}$  and Al 11.4  $\mu\text{m}$ . As discussed in Section 3.2, additional data taken in two other softer filters, Al1 and AlMg, are included to analyze flare 4. The SXT data have been processed according to the standard Yohkoh Analysis System. The datasets consist of sequences of frames  $64 \times 64$  pixels of 2.5 arcsec side, taken alternatively in the two filter bands, with sampling cadence usually ranging between  $\sim 10$  sec (typically in the rise phase and around the flare peak) and  $\sim 60$  sec in late decay phase of long-lasting flares.

The analysis then includes the derivation of temperature and EM maps, as in Papers I and II, during the flare evolution. Since the plasma conditions may change significantly in the time taken to switch between the two filters, , the data in the Al 11.4  $\mu\text{m}$  filter band have been interpolated to the exact times of the Be 119  $\mu\text{m}$  data (as done routinely in the standard Yohkoh data analysis), in order to improve the accuracy of the temperature and emission measure estimates.

The distributions of EM vs T (EM(T)) are then derived from the T and EM maps with the procedure illustrated in Paper I and II. In any of the two filter bands we have screened out saturated pixels, typically in the brightest regions, and pixels which collected photons below a threshold of 10 photons. These pixels would introduce large errors and are therefore critical in the analysis of EM vs T for localized events like flares. We have carefully

selected for our analysis only those frames with no (or just very few) saturated pixels. The temperature bins for the EM( $T$ ) are those defined in Papers I and II, i.e. 29 bins uniform in  $\log T$  between  $\log T = 5.5$  and  $\log T = 8$ .

## 2.2. From the EM( $T$ ) distribution to the stellar-like spectra

From each of the several EM( $T$ ) distributions of a flare obtained during its evolution we synthesize the relevant X-ray spectrum with the MEKAL spectral code (Kaastra 1992; Mewe et al. 1995), and filter it through the instrumental response of non-solar telescopes of interest. The process to generate the stellar-like spectra from an EM( $T$ ) distribution derived from the solar data is described in Paper II. Metal abundances are assumed as in Anders & Grevesse (1989).

In this paper, we consider the stellar-like focal plane spectra that *ASCA*/SIS and *ROSAT*/PSPC would collect, observing the solar flares selected here at stellar distances. It would be very interesting to perform finely time-resolved spectroscopy, but in real stellar observations this is prevented by the limited counting statistics of the source. Analogously to stellar observations, therefore, the flare spectra have to be integrated on time intervals of hundreds of seconds to increase the overall statistics of the fitting process. This means that the flares are binned into few time intervals. Since flares evolve on time scales smaller or of the same order, the data collected in a time bin do not represent steady plasma conditions but integrate on significant variations of the plasma temperature and density in the same dataset. Therefore when time-resolved flare data are analyzed with steady-state models, one should keep anyhow in mind that this is an *a priori* limited representation and description of the data. In order to approach the typical conditions of non-solar flare observations we make the following exercise:

1. we sample the EM( $T$ )'s of a flare at constant time intervals of 60 sec
2. from each EM( $T$ ) we synthesize the corresponding spectrum filtered through the spectral response and effective area of two instruments, namely *ASCA*/SIS and *ROSAT*/PSPC
3. we bin the flare into three (or more) long time segments, (at least) one including the rise phase, one the flare maximum and one the decay phase. The duration of the time segments varies within each flare and from flare to flare, depending on the flare duration and on the data structure (the presence of gaps, for instance), and span from a minimum of 180 s to a maximum of  $\sim 3000$  s.

4. each spectrum is normalized so as to yield a total number of counts in each time interval typical of good stellar flare observations (e.g. between 1000 and 10000 counts for ASCA); to this end we have to assume the distance at which the solar flare would yield the appropriate statistics. We randomize the photon counts according to Poisson statistics
5. we sum all folded and randomized spectra within each time bin and therefore obtain a single spectrum for each time bin.
6. we analyze each spectrum with the standard thermal models used for stellar data analysis.

We apply the standard stellar analysis to the binned spectra and use the tools commonly used by the stellar community. In particular, we fit the stellar-like spectra with multiple-isothermal components models. In the ROSAT/PSPC case, we exclude channels with less than three counts from the analysis to grant an appropriate evaluation of  $\chi^2$ , and the first two channels because they are typically affected by systematic errors. In the ASCA/SIS case, the energy channels are grouped so to have at least 20 photon counts per channel; furthermore the channels with bad quality or empty are discarded<sup>1</sup>. We use the X-ray spectral fitting package XSPEC V10.0 and the manipulation task FTOOLS V4.0. Most fittings are performed with single temperature components, assuming negligible column density  $N_H = 0$ , and standard metal abundances kept fixed. Some checks have been done by allowing metal abundance to vary all by the same amount.

### 3. Results

#### 3.1. Flare properties

All flares listed in Table 1 last between 9 and 90 min, except the huge flare 8, of class X9, whose duration is more than 6 hours (despite the GOES log reports less than 1 hour). The SXT observation of flare 8 is divided into 3 segments separated by two gaps lasting more than one and two hours, respectively. The first segment begins just around the flare maximum, and therefore most of the flare rise phase is not covered by SXT. We have selected anyhow this flare because it is a rather extreme case of intense flare and the information from the rise phase is not crucial for our findings, as described below.

---

<sup>1</sup>The first 18 channels of ASCA/SIS below 0.5 keV are discarded because they are affected by systematic errors.

In all the other cases the related SXT observation covers quite well both the rise and the decay phase and the flare maximum is well within the observation. Only for flare 7 (class X1.5) the decay phase is monitored for a relatively short time.

As part of our analysis we investigate the role of the morphology of the flaring region in determining the  $EM(T)$ , and the effect of the heating release, and in particular of its intensity, duration and decay time, on the evolution of the  $EM(T)$ . In this perspective we tag each flare with the light curve in both filters of SXT flare-mode, its path in the density-temperature (hereafter  $n$ - $T$ ) diagram (the square root of the emission measure is used as proxy for the density), and the main morphological features observable in the SXT images. Fig. 1 and Fig. 2 show the light curves in the Al 11.4  $\mu\text{m}$  and Be 119  $\mu\text{m}$  filter bands obtained by summing all the counts in each 64x64 pixels SXT frame, and the corresponding  $n$ - $T$  diagrams, obtained from the ratio of the light curves data points. Notice that the resulting temperature is a weighted average temperature of the whole region in each frame.

Flare 2 is particularly well-covered since the total luminosity at the end has decayed to the values at the beginning; this corresponds to a closed cycle in the  $n$ - $T$  diagram. The  $n$ - $T$  diagram also shows that this is the only flare in which the temperature changes significantly during the rise phase (from  $\log T \approx 6.8$  to  $\log T \approx 7.1$ ). This may indicate that the heating which triggers the flare is released more gradually in the rise phase of this flare than in the others (e.g. Sylwester et al. 1993). During the other six flares for which the rise phase has been observed, the temperature is in fact much more constant and stays above  $10^7$  K during the rise phase. As for the density, Yohkoh/SXT has detected an increase of more than half a decade of  $EM^{1/2}$  for five flares (flare 2, 4, 5, 6 and 7); during the decay of flare 8 the decrease of  $EM^{1/2}$  is particularly significant, i.e. almost one order of magnitude.

Table 2 shows relevant physical and morphological characteristics of the selected flares obtained with the flare mode filters, i.e. the slope of the flare decay path in the  $\log(EM^{1/2}) - \log(T)$  diagram, the decay time of the light curve in the Al 11.4  $\mu\text{m}$  filter band (the latter two quantities are used to estimate the flaring loop length according to Reale et al. 1997), conservative loop half-length ranges obtained from measuring the loop projections on the images and from applying the method of Reale et al. (1997), the morphology of the flaring region (Fig. 3 shows one grey-scale image sampled during each flare), the maximum temperature and emission measure obtained with the filter ratio method from the ratio of the data points of the light curves in the two flare-mode filter bands. The slope  $\zeta$  is an indicator of sustained heating during the decay, whenever significantly smaller than  $\sim 1.7$  (Sylwester et al. 1993).

From Table 2 we see that:



- Heating is negligible during the decay of three flares (1, 3 and 6), significant during the decay of the other five and in particular of the most intense ones (7 and 8). The slope  $\zeta$  of the whole decay of flare 8 is below the minimum possible value ( $\zeta_{min} \approx 0.3$ ) predicted by single loop hydrodynamic modeling (Reale et al. 1997), which means that this model is not applicable in this case, and that, therefore, significant magnetic rearrangements and complicated and continued heating release probably occur.
- The light curve e-folding decay time is below 30 min for all flares except flare 4, an arcade flare, and flare 8.
- The loop half-length is in the range 10 Mm and 100 Mm, typical of active region loops<sup>2</sup>.
- The morphology of the flaring regions ranges from simple single loops to multiple loops, an arcade and even more complicated structures.
- The maximum values of the average temperatures, as measured with Yohkoh filter-band ratio, are in the range  $7.1 \leq \log(T) \leq 7.3$ , weakly increasing with the GOES class.
- The maximum total emission measure increases with the flare GOES class and spans two orders of magnitudes from  $10^{49}$  to  $10^{51} \text{ cm}^{-3}$ .

The above considerations make us confident that this sample of flares is enough representative of flare conditions typically met on the Sun and can be used to derive general properties to be compared to those observed in stellar flares.

### 3.2. Flare EM(T)

Fig. 4 shows the evolution of the EM(T) obtained with the two hardest SXT filters, during the eight selected flares<sup>3</sup>. For each flare we show the emission measure distributions sampled at a constant rate of one every 2 min since the beginning of the data selected as in Section 2. The longer the flare, the more are the EM(T)'s shown: those shown for the short flares 1 and 7 are much fewer than those shown for flare 8, by far the longest one. For reference, Fig. 4 shows also the EM(T)'s obtained in Paper II for the Sun near the maximum and the Sun near the minimum of the cycle.

---

<sup>2</sup>Since flare 4 is an arcade flare, it involves bundles of loops and the loop length in Table 2 is to be taken as an indicative scale size.

<sup>3</sup>For the sake of clarity, the flare EM(T)'s are not shown as histograms.

Fig. 4 shows that at any flare phase the EM(T) is typically quite narrow, practically independent of the flaring region morphology, and covers a temperature decade around  $\sim 10^7$  K. It is much narrower than any EM(T) of the whole Sun. Exceptions are the EM(T)'s obtained for flare 8, the most intense one, which shows significant amounts of hotter plasma, at temperatures up to  $\sim 10^8$  K. The EM(T) reaches for this flare maximum values  $> 10^{50}$  cm $^{-3}$ . Hot plasma at temperatures above 30 MK is present in flares more intense than M1.1 (flare 3).

In Fig. 4 the EM(T) of all flares clearly follows a common evolution path: it starts low but already at a relatively high temperature, centered at  $\sim 10^7$  K; it grows toward higher EM values, maintaining a more or less constant shape and sometimes shifting slightly rightwards to higher temperatures (e.g. flares 2, 4 and 6); then it decays by gradually cooling (leftwards) and decreasing (downwards). We can clearly identify envelopes of the evolving EM(T)'s and notice that the slope of the envelopes in the decay phase (determined by the relative rate of the emission measure decrease and the temperature decrease) is linked to the slope in the n-T diagram (see Fig. 1 and Fig. 2). Several EM(T) distributions late during the decay are partially hidden by the higher preceding ones (e.g. flares 3, 4 and 5). This clearly shows that the EM(T) mostly evolves inside a “common envelope” in the rise and the decay phase, with important implications on the interpretation of some stellar coronal EM(T)'s (see Section 4).

The EM(T)'s shown in Fig. 4 are derived from observations in the hardest SXT filters bands. Since these filters are most sensitive to plasma around and above  $10^7$  K, one may wonder whether contributions from plasma at lower temperatures, not detected by the two filters, may be important to the flare EM(T), or not. The observation of flare 4 includes several frames taken in the Al.1 and AlMg filter bands and allows us to investigate this item. Fig. 5 shows the EM(T)'s of flare 4 at the same times as those shown in Fig.4, but including contributions to the EM(T)'s derived from images in the softer filters bands mentioned above. Cooler contributions to the EM(T)'s are clearly present from comparison with Fig.4. These contributions make each EM(T) flatter at temperatures below the EM(T) maxima ( $\sim 10^7$  K); the slope in this rising region approaches the  $T^{3/2}$  trend expected from loop structures (see Peres et al. 2001).

Although the presence of such contributions modify the shape of the EM(T)'s in the low temperature part, they are anyhow significantly smaller than the dominant components around  $10^7$  K, and we have checked that the analysis of stellar spectra synthesized from EM(T)'s with and without such contributions does not change significantly, as further discussed in Section 3.3. Since very few flares yielded good data in softer filters bands (saturated pixels are much more frequent), and contributions from such bands are anyhow affected by uncertainties and contaminations from the coexistence of cool and hot plasma within the

same pixel, we prefer to perform the analysis considering expositions only in the two hardest filters and keeping anyhow in mind the limitations that this choice implies.

All EM(T)’s obtained for flares are well separated and distinct from the EM(T) of the Sun at minimum. They are also mostly “higher” than the EM(T) of the Sun at minimum. The EM(T)’s of the first three flares are instead all lower than the EM(T) of the Sun at maximum, while the EM(T)’s of the remaining five flares are comparable or higher. If we did the exercise, similar to that in Paper II, to build a single EM(T) of the flaring Sun at maximum by combining that of the Sun at maximum and any one of the latter flares, we would invariably obtain an EM(T) with two distinct peaks, the hotter one being associated with the flare. Flare 8 involves emission measures quite higher than the emission measure of the full non-flaring Sun at maximum (see Paper II).

Fig. 6 shows the maxima of the EM(T)’s of all of the eight flares. This figure indicates that an increasing intensity in the GOES class mostly corresponds to an increase in the EM(T) height and much less to an increase in temperature and/or in the EM(T) width. An exception is flare 8 which is significantly hotter and wider.

### 3.3. Flare spectra

From each EM(T) obtained during the flares we can synthesize the corresponding X-ray parent spectra for an optically thin plasma in thermal equilibrium, as described in Paper II. Fig. 7 shows examples of X-ray spectra in the 0.2-20 keV band, synthesized from EM(T) at the beginning, peak and end of Flare 2 and at the peak and data end of Flare 8. The maximum luminosities in the whole band result to be  $\approx 3.5 \times 10^{26}$  erg/s and  $\approx 1.3 \times 10^{28}$  erg/s, respectively. From Fig. 7 we see concentrations of emission lines around 1 keV, typical of plasma mostly at temperature around  $10^7$  K, and mostly due to the Fe-L complex. The spectrum at the peak of flare 8 shows prominent lines of the Fe group at energies around 6 keV, which are sensibly reduced at the end of the data (lower panel, dashed line). Notice that the continuum of the spectrum at the peak of flare 8 is considerably flatter than the others shown and indicates that there are contributions of plasma at significantly hotter temperatures than in all other synthesized spectra shown.

#### 3.3.1. ASCA/SIS spectra

Fig. 7 shows ASCA/SIS spectra of flare 4. These spectra have been analyzed by fitting them with spectral models consisting of one isothermal plasma component (*1-T fit*). Table 3

shows the results of the spectral analysis applied to four of the eight selected flares (2, 4, 6, and 8). For each flare, the Table includes the distance at which we put the flaring Sun, and, for each time bin, the phase of the flare it covers, the time range, the number of counts, the best-fit temperature and emission measure, the number of degrees of freedom (the number of energy channels yielding a significant number of counts minus the parameters of the fitting) and the reduced  $\chi^2$  of the fitting.

Table 3 tells us, first of all, that the single thermal component model already provides an acceptable description of the various phases of the flares, in agreement to the rather peaked EM(T) distributions that we obtain from the two hard SXT filters, even averaging over each time bin. In spite of the fast flare evolution, temperature and emission measure variations *within* each time bin do not affect the 1-T fitting in the rise phase, mainly for two reasons: i) the emission measure at the end of the bin in the rise phase is much higher than, and dominates over, that at the beginning; ii) generally the temperature does not vary much during the rise phase. Conditions are quite stable during the flare maximum and a single temperature therefore describes reasonably well this phase.

On the contrary, in spite of the relatively slow evolution, during the decay plasma temperature may vary significantly from the beginning to the end of the same time bin, while the emission measure remains relatively constant (or slowly decreasing). The single temperature component may therefore fail to describe time bins of the decay phase, especially in flares with a steep slope in the n-T diagram. Indeed in bins e) and f) in the decay phase of flare 6, the fitting is not as good ( $\chi^2 > 1.7$ ) as in the other ones or in the other flare decays: the slope of the decay of this flare in the n-T diagram is very high ( $\zeta > 1.7$ ), higher than in all the other flares. 1-T fitting of spectra taken with ASCA during stellar flare decays, and subtracted of the spectrum of the background non-flaring corona, have sometimes failed (e.g. Favata et al. 2000), and our results suggest a possible explanation.

The best-fit temperature values approximately correspond to the maxima of the EM(T) distribution averaged in the respective time bin and the corresponding emission measure values are approximately proportional to the total emission measure in that bin. The maximum emission measure values are slightly smaller than the values listed in Table 2, both because some contributions are excluded by the instrument limited spectral band and because in the respective time bins of Table 3 the emission measure is not constantly at maximum. Notice that due to scaling with respect to the maximum, the last bin of flare 8 yields only 400 photon counts, since the emission measure is two orders of magnitude smaller than at maximum.

The last section of Table 3 reports again results for flare 4 but including the components obtained from the softer filters (see Fig.5). Comparing to the results without the softer

filters, we notice the slightly higher count statistics, the slightly lower best-fit temperature, the slightly larger emission measure, the generally higher  $\chi^2$ . The higher  $\chi^2$  indicates that the single thermal model is not as good as previously, but not to such a point to discriminate the presence of the cooler components, also considering the higher count statistics.

Finally, we have checked the effect of fitting the simulated ASCA data with 1-T models in which the global metal abundance is left free to vary, from one spectrum to the other. The resulting best-fit abundance values are generally different from the expected solar value and vary within a factor two, either in excess or in defect, from the central unity value. In the course of a flare we obtain either abundances all smaller than one, or all larger than one, or fluctuating around one. Although in a few cases the abundance appears to decrease during the decay, we were not able to identify clear systematic trends of abundance variations during the flare evolution. The best-fit  $\chi^2$  values are improved by 0-10%, and in no case by more than 20%, while the temperature values are practically unchanged (while the emission measure values vary in inverse proportion to the abundance values). The detection of such abundance variations are clearly an artifact of the model fitting process, since the synthesized spectra are consistently built by assuming fixed solar metal abundances at any step and can be explained in the following terms: the EM(T) flare distributions are neither sharp enough to be described at best by a simple  $\delta$  function (an isothermal model), nor broad enough to require a multi-thermal (e.g. 2-T) model. Moderate abundance variations are sufficient to account, and adjust the fit, for the presence of minor emission measure components around the dominating maximum component. This exercise tells us that although the limited broadness of the flare EM(T) may favor an improvement of spectral fitting by letting abundance vary, the resulting abundance variations seem to be random; therefore we cannot exclude that systematic abundance variations are to be explained by effects other than the one illustrated here.

### 3.3.2. *ROSAT/PSPC spectra*

ROSAT/PSPC has a lower spectral resolution than ASCA/SIS, and is, therefore, less able to discriminate multi-thermal components. In fact, we find that a single thermal component model describes even better the PSPC spectra obtained from the flare EM(T)'s averaged over the same time bins as those used for ASCA/SIS. We have analysed spectra yielding a maximum between 3000 and 5000 total counts: all fittings were acceptable (reduced  $\chi^2 < 1.5$  with less than 30 degrees of freedom). The temperature and emission measure values are very similar (with a mean deviation within 10% and 15%, respectively) to those obtained with ASCA/SIS spectral fitting. On the average, the ROSAT temperature is slightly system-

atically lower ( $\sim 3\%$ ) than the corresponding ASCA one, and the emission measure slightly higher ( $\sim 1\%$ ).

Analogously to Paper II, as an additional piece of analysis of the synthesized ROSAT/PSPC data, we compute the surface X-ray flux  $F_X$ , defined as the X-ray luminosity in the ROSAT/PSPC spectral band divided by the pixel area over which the Yohkoh/SXT photon count is larger than 10 cts/s, and the hardness ratio defined as in Schmitt (1997):

$$HR = \frac{H - S}{H + S} \quad (1)$$

where  $S$  are the total counts in the (soft) PSPC sub-band 0.13-0.4 keV and  $H$  are the total counts in the (hard) sub-band 0.55-1.95 keV.

Fig. 8 shows  $F_X$  vs HR for each time bin in which a spectrum has been collected, and for all flares. All data points appear to lie in a relatively thin vertical strip around a hardness ratio value of 0.3 and with  $F_X$  ranging from  $10^6$  to  $10^9$  erg cm $^{-2}$  s $^{-1}$ . The smallest flares evolve mostly in the range  $10^7$  to  $10^8$  erg cm $^{-2}$  s $^{-1}$ , while the most intense ones seem to move in a wider flux range. The flare evolution has no well defined trend in this plane, mostly because of the very limited variation of the hardness ratio. The almost constant HR is mostly due to two factors: i) the flare average temperature, of which the hardness ratio is a proxy, does not change much from  $T \sim 10^7$  K, during the flare evolution; ii) the hardness ratio, as defined above, is weakly sensitive to temperature variations (and even multi-valued) around  $T \sim 10^7$  K. For comparison, Fig. 8 shows the plane region occupied by late-type stars observed by ROSAT/PSPC (Schmitt 1997): solar flares (isolated from the remaining corona), practically in any phase of their evolution, are harder than typical stellar coronal emission and in a region of high surface flux.

#### 4. Discussion

Papers I and II illustrated a method to use the Sun as a template of X-ray stars, converting Yohkoh/SXT solar data into corresponding focal plane data collected by non-solar telescopes, such as ROSAT and ASCA, from a Sun located at stellar distances. This work presents the application of this method to solar flares. In order to sample the various flare conditions, we have selected a set of flares spanning from weak to extremely intense and occurring either in simple loop structures, or in complex regions or arcades. The method is, in general, the same as that used to analyse the full-disk non-flaring observations. However some important differences are in order:

- Yohkoh SXT flare observations are performed with different characteristics, the so-called flare-mode, which involves mostly the use of two harder filters, double (full) spatial resolution and a much higher sampling cadence.
- Flares evolve on short time scales and the evolution of the emission measure distribution is a mostly important item of the present study.
- Flares are highly localized in areas of the order of 1/1000 of the solar hemisphere; although their luminosity is often comparable to that of the whole corona, their evolution is mostly independent of what happens in the rest of the corona, and we study them as self-standing phenomena also from the stellar point of view.

The two flare-mode filters are mostly sensitive to plasma at temperatures above  $10^7$  K, appropriate for flares; however their sensitivity to plasma below  $10^7$  K is low, and temperature and emission measure diagnostics are not at best. Since the plasma is typically stratified inside coronal structures, even during flares, we may then miss contributions from relatively cool plasma components which may be significant, or even dominant, or coexisting with hotter plasma, in some pixels during the flare evolution. The presence of such a cooler plasma has indeed been detected in a flare observed both with flaring mode filters and with standard mode filters (flare 4): the emission measure distribution during the evolution is not modified for  $T \geq 10^7$  K but additional (lower) contributions appear for  $T < 10^7$  K making the EM(T) less steep on the cool side of the maximum. This should be kept in mind when discussing the shape of the EM(T) distributions. The slope of the cool side approaches 3/2, the typical value expected for standard loop structures in equilibrium (see also Peres et al. 2001), coherently to flare evolution being dominated by plasma confined in closed magnetic structures and suggesting that, after the initial (not bright) impulsive phases, the dynamics is significantly less important and the flaring plasma is very close to equilibrium conditions.

We notice that the shape and evolution of the EM(T) during flares little depend on the detailed geometry of the flare region, as well as on the flare intensity (except, of course, for the relative EM(T) height): in Fig.3 one can hardly distinguish flare 4, an arcade flare, and flare 8, very intense and complex, from the other flares with simpler geometry. Flare 4 and flare 8 last longer than the others, and their temperature decreases very slowly, but these features are not evident in Fig.3. The temperature of the EM(T) maximum is also weakly dependent on the flare intensity: this may depend in part on the flare-mode filters used, which are more sensitive to plasma around that temperature, but also on the strong efficiency of thermal conduction ( $\propto T^{5/2} \nabla T$ ) at higher and higher temperature, which implies a very large energy input even for a small temperature increase, to balance conductive losses to chromosphere.

Significant amount of plasma at very high temperature ( $\lesssim 10^8$  K), comparable to the peak temperatures of intense stellar flares, is detected, in particular during flare 8. Such hot plasma, however, has an overall low emission measure with respect to the dominant relatively cooler plasma at  $T \sim 10^7$  K. Our results show that minor components of emission measure hotter than the dominant component described by the single temperature fitting are practically not detectable in low resolution spectra collected by ROSAT and ASCA during stellar flares. High resolution spectra collected by Chandra and Newton may show them (Fig.6).

ROSAT and ASCA spectra synthesized from our EM(T)'s, even integrated over long time segments and at relatively high count statistics, are well-fitted by single isothermal components, at or around the temperature of the EM(T) peak. Even when we include additional cooler contributions obtained from the softer SXT filters, 1-T fit is successful, albeit at a slightly lower best-fitting temperature. Deviations from isothermal behavior in ROSAT and ASCA synthesized spectra are sometimes obtained in the decay phase because of variations of plasma temperature within the same time segment.

These results can be used to interpret observations of stellar flares: successful isothermal fittings of time-resolved spectra (such as those mentioned in Section 1) detect the dominant component of a multi-component but single-peaked emission measure distribution, and the distributions of the solar flares presented here may be taken for reference. High  $\chi^2$  values during the decay may not be indicative of a multi-temperature distribution of the flaring region, rather of the evolving temperature of the dominant emission measure component.

We also notice that the single component fittings, both of ROSAT and ASCA spectra, generally well evaluate the total emission measure involved, missing only few percent of the parent emission measure. Therefore the emission measure values obtained from the fittings are rather reliable.

Our approach does not allow us to address exhaustively the problem of metal abundance variations obtained to best-fit the spectra of several stellar flares; however we made the exercise to fit the stellar-like solar spectra letting the global metal abundance free to vary. We have found that non-solar abundances help to improve somewhat the fitting quality, probably because they better account for the limited broadness of the flare EM(T)'s, but they do not seem to vary systematically (e.g. increase first and then decrease in the decay) during each flare. Therefore, we cannot exclude that the evidence of systematic abundance variations requires explanations different from the one suggested by our results.

The analysis of the ROSAT/PSPC flare simulated spectra tells us that the solar flares group in the X-ray flux vs hardness ratio diagram, and in particular in a narrow strip



spanning two orders of magnitude at relatively high flux values and hardness ratio value between 0.2 and 0.5. This strip is rightwards (harder), in practice completely outside, of the region occupied by the G stars sampled by Schmitt (1997), which however pertain to whole coronae, outside flares. This is consistent with both flux and hardness ratio of non-flaring solar-like stellar coronae being well below conditions of typical solar flaring regions, which also agrees with the range of temperatures seen in non-flaring stars vs. stellar or solar flares.

We now discuss some major implications of our results on the analysis of stellar coronae. There is evidence that the emission measure distribution of very active stellar coronae, obtained from spectrally resolved XUV observations, is double-peaked; the first peak is at a few  $10^6$  K, and the second peak above  $10^7$  K (Griffiths and Jordan 1998). This aspect is much debated and still open, but it has been suggested that this hot component may be due to continuous flaring activity (Güdel 1997, Drake et al. 2000): the stellar surface is covered by active regions, flares are very frequent and their light curves overlap, cancelling out any variability due to the single events. In this framework, the present work shows that a double-peaked EM(T) distribution is indeed obtained if one combines the EM(T) of the whole corona to the envelope of the EM(T)'s during the flares (see Fig. 3). The two peaks are clearly evident also when summing the EM(T)'s of flares from 4 (M2.8) to 8 (X9) to the EM(T) of the Sun at maximum of its cycle of activity. This seems to suggest that uninterrupted sequences of overlapping proper flares, whichever their evolution, would not be able to fill the gap between the two EM(T) peaks, which, therefore, would be a permanent feature of the EM(T) of an active star.

Indeed this second distinct maximum associated with flares is not surprising also on the basis of theoretical modeling. From hydrodynamic modeling of flaring plasma confined in magnetic loops, it has been generally found that the impulsive heating originating the flare first causes a very fast local temperature enhancement above  $10^7$  K which propagates along the whole loop in few seconds due to the highly efficient (even in saturated regimes) thermal conduction. The loop plasma density (and therefore emission measure) increases more slowly and gradually, because determined by evaporation of plasma up from the chromosphere, on typical dynamic time scales (minutes). Later, when heating decreases, temperature and density both decay, their relative decay rate dictated by the rate of the heating decrease. *Models never predict that temperature does decrease and density does not*, which would result into an emission measure distribution maintaining the bell-shape, with little or no change of shape and shifting from high to lower temperature, thus filling the gap between the two EM(T) peaks. This scenario would be at variance with both hydrodynamic models and observations as represented in the density- temperature diagrams shown in Fig.1: for all flares except flare 2 the temperature is high and the emission measure low (upper left extremes of the paths) already at the beginning of the observation. In the decay the path is

never vertical (i.e. maintaining a constant EM and decreasing T), but has a maximum slope (theoretically found to be less than 2, Jakimiec et al. 1992). All this means that the EM(T) during flares, whatever its exact shape, will:

1. increase starting already from  $\sim 10^7$  K
2. cool but also invariably decrease, in the flare decay. The cooling may be much slower than the decrease, if the heating is sustained during the decay, as it seems to occur in many flares (Sylwester et al. 1993, Reale et al. 1997).

These considerations and results, in our opinion, show that a major continuous flaring activity on a stellar corona would produce an EM(T) with two distinct peaks, the higher temperature one at  $T \geq 10^7$  K; the peak will be sharper if flares are heated during their decay.

## 5. Conclusions

This work provides a key to interpret stellar flare X-ray data in terms of solar ones. In particular: it provides templates of stellar flare spectra and it tells us that the single thermal components which typically fit stellar flares low-resolution spectra are in agreement with single peaked, relatively sharp, emission measure distributions vs temperature. Our simulations indicate that the best-fit temperature of flare spectra collected with ROSAT/PSPC and ASCA/SIS corresponds to the maximum of the flare EM(T), and that the emission measure values obtained from the fitting well reproduce the total parent emission measures. This work also allows us to put solar flares in relationship with the surface emission of stellar coronae and explains why a continuous, moderate, flaring activity may produce a second peak in the emission measure distribution vs temperature.

We expect more detailed information, such as the detection of minor emission measure components at very high temperatures, from high resolution spectra of stellar flares collected by Chandra and XMM/Newton.

This work was supported in part by Agenzia Spaziale Italiana and by Ministero della Università e della Ricerca Scientifica e Tecnologica.

## REFERENCES

- Anders, E., Grevesse, N., 1989, *Geochimica et Cosmochimica Acta*, 53, 197.
- Brinkman, A.C., et al., 2001, *A&A*, 365, L324.
- Drake, J.J., Peres, G., Orlando, S., Laming, J.M., Maggio, A., 2000, *ApJ* in press
- Favata, F., Reale, F., Micela, G., Sciortino, S., Maggio, A., Matsumoto, H., 2000, *A&A*, 353, 987.
- Gotthelf, E.V., Jalota, L., Mukai, K., White, N.E., 1994, *ApJL*, 436, L91
- Griffiths, N.W., Jordan, C., 1998, *ApJ* 497, 883
- Güdel, M., 1997, *ApJ*, 480, L121.
- Güdel, M., Linsky, J. L., Brown, A., Nagase, F., 1999, *ApJ*, 511, 405
- Hamaguchi, K., Terada, H., Bamba, A., Koyama, K., 2000, *ApJ*, 532, 1111
- Jakimiec, J., Sylwester, B., Sylwester, J., et al. 1992, *A&A*, 253, 269.
- Kaastra, J. S., An X-ray Spectral Code for Optically Thin Plasmas, Internal Report, updated version 2.0 (SRON - Leiden).
- Maggio, A., Pallavicini, R., Reale, F., Tagliaferri, G., 2000, *A&A*, 356, 627.
- Mewe, R., Kaastra, J. S., Liedahl, D.A., 1995, *Legacy*, 6, 16.
- Orlando, S., Peres, G., Reale, F., 2000, *ApJ*, 528, 524 (Paper I)
- Osten, R. A., Brown, A., Ayres, T. R., Linsky, J. L., Drake, S. A., Gagnè, M., Stern, R. A., 2000, *ApJ*, 544, 953
- Ottmann, R., Schmitt, J.H.M.M., 1996, *A&A*, 307, 813
- Peres, G., Orlando, S., Reale, F., Rosner, R., Hudson, H., 2000a, *ApJ*, 528, 537 (Paper II)
- Peres, G., Orlando, S., Reale, F., Rosner, R., 2001, *ApJ*, submitted
- Preibisch, T., Zinnecker, H., Schmitt, J.H.M.M., 1993, *A&A*, 279, L33
- Reale, F., Betta, R., Peres, G., Serio, S., McTiernan, J., 1997, *A&A* 325, 782
- Reale, F., Micela, G., 1998, *A&A*, 334, 1028
- Reale, F., Peres, G., 1995, *A&A*, 299, 225
- Schmitt, J. H. M. M., 1997, *A&A*, 318, 215.
- Schmitt, J. H. M. M., Favata, F., 1999, *Nat.*, 401, 44
- Serio, S., Reale, F., Jakimiec, J., Sylwester, B., Sylwester, J., 1991, *A&A*, 241, 197.
- Sylwester, B., Sylwester, J., Serio, S., et al., 1993, *A&A*, 267, 586.

Tsuboi, Y., Imanishi, K., Koyama, K., Grosso, N., Montmerle, T., 2000, ApJ, 532, 1089  
van den Oord, G.H.J., Mewe, R., Brinkman, A.C., 1988, A&A, 205, 181.  
van den Oord, G.H.J., Mewe, R., 1989, A&A, 213, 245.

Fig. 1.— Yohkoh/SXT light curves and density-temperature diagrams for the first four of the eight flares listed in Table 1. Two light curves are shown for each flare: the one in the Be 119  $\mu\text{m}$  filter band and the other in the Al 11.4  $\mu\text{m}$  filter band. The square root of the emission measure is used as a proxy of the average density.

Fig. 2.— As in Fig.1 for the remaining four of the eight flares listed in Table 1.

Fig. 3.— Grey scale pictures of the flaring regions as imaged by Yohkoh/SXT in the Al 11.4  $\mu\text{m}$  filter band. The grey scales on the bottom left of each picture are in Data Number (DN). The position of the field of view on the solar disk is indicated in low right corner of each image.

Fig. 4.— Evolution of the EM(T) during the eight selected flares. The emission measure distributions are sampled every  $\approx 2$  min since the beginning of the valid data. The time sequence goes from lighter to darker grey shaded profiles. Examples of the EM(T)'s obtained in Paper II for the Sun at maximum (solid histogram) and at minimum (dashed histogram) of the solar cycle are also shown for reference (from Peres et al. 2000a). The vertical dashed line marks  $10^7$  K.

Fig. 5.— Evolution of the EM(T) during Flare 4, as in Fig.4, including EM contributions derived from observations in two softer Al.1 and AlMg filter bands.

Fig. 6.— EM(T)'s yielding the maximum total emission measure of the eight flares. Lighter to darker grey shaded profiles mark flare 1 to 8 in Table 1. Reference histograms and vertical line as in Fig. 4.

Fig. 7.— Examples of solar X-ray spectra in the 0.2-10 keV band synthesized from EM(T)'s at an early phase, peak and end of Flare 2 (left panels) and at the peak and data end of Flare 8 (right panels). The top panels show the parent spectra, the middle panels the spectra as they would be detected by ROSAT/PSPC and the bottom panels as they would be detected by ASCA/SIS at stellar distances. In each panel of the ROSAT/PSPC and ASCA/SIS spectra, the simulated data (crosses) are shown together with the best-fit one-temperature MEKAL spectra (solid histograms) derived from the analysis (see Table 3).

Fig. 8.— X-ray surface flux vs hardness ratio in the ROSAT/PSPC band obtained for various phases of the solar flares. Each data point is derived from the PSPC spectrum of the EM(T)'s studied with the standard methods used for stellar data. (see Table 3). The dashed line envelopes the stellar data reported in Schmitt (1997).

Table 1: Selected solar flares

N.	Date <sup>a</sup>	GOES Class	Duration <sup>b</sup> (min)	Start Time <sup>c</sup>	Time of EM <sup>d</sup> <sub>max</sub>	End Time <sup>c</sup>
1	920718-0505	C5.8	9	05:08	05:12	05:18
2	930210-0734	M1.0	12	07:35	07:42	08:03
3	921019-1751	M1.1	20	17:54	18:00	18:28
4	940227-0825	M2.8	86	09:03	09:25	09:47
5	911226-2133	M4.2	30	21:35	21:45	21:55
6	920206-0311	M7.6	92	03:16	03:31	03:46
7	911115-2233	X1.5	21	22:35	22:38	22:44
8 <sup>e</sup>	921102-0231	X9.0	57	03:04	03:08	03:35
				04:42		05:38
				07:57		08:52

<sup>a</sup> YYMMDD-HHMM of the flare beginning as reckoned by GOES

<sup>b</sup> As in GOES log file

<sup>c</sup> Start and end time of the Yohkoh/SXT observation

<sup>d</sup> maximum of the total emission measure obtained summing over all the pixels in each SXT frame

<sup>e</sup> The observation is split into three segments

Table 2: Parameters of the selected solar flares

N.	$\zeta^a$	$\tau_{Al}^b$ (sec)	$L^c$ $10^9$ cm	Morphology <sup>d</sup>	$\log(T_{max})^e$	$\log(EM_{max})^e$
1	> 1.7	260	2-3	1 Loop	7.10	49.1
2	0.8	330	1-2	Complex	7.13	49.2
3	1.6	1300	5-10	1 Loop	7.12	49.3
4	0.8	3700	> 10	Arcade	7.12	49.9
5	0.9	1100	5	2 Loops	7.15	49.8
6	> 1.7	1800	> 5	2 Loops	7.19	50.0
7	0.6	660	2-3	1 Loop	7.18	50.4
8	0.2	5800	> 5?	Complex	7.28	51.0

<sup>a</sup> Slope in the n-T diagram (Reale et al. 1997)

<sup>b</sup> Decay time of the light curve in the Al 11.4  $\mu$ m filter

<sup>c</sup> Ranges of loop half lengths estimated from the SXT images and from the method in Reale et al. (1997).

<sup>d</sup> From a visual analysis.

<sup>e</sup> maximum of the weighted average temperature and total emission measure in each frame

Table 3: Results of 1-T fitting of ASCA spectra of solar flares

Flare	Dist. <sup>a</sup> (pc)	Bin	Phase <sup>b</sup>	Bin time range <sup>c</sup> (sec)	cts	T <sub>best</sub> (10 <sup>7</sup> K)	EM <sub>best</sub> (10 <sup>49</sup> cm <sup>-3</sup> )	Chan.	$\overline{\chi^2}$
2	0.05	a	R	0-180	3300	1.14	0.54	45	1.4
		b	R	180-360	6900	1.26	1.1	65	1.3
		c	M	360-540	8200	1.00	1.1	56	1.5
		d	D	540-900	5400	0.77	0.35	43	1.3
4	0.3	a	R	0-500	660	1.18	1.3	19	0.9
		b	R+M	500-1000	2300	1.19	4.6	41	0.9
		c	M+D	1000-1500	3400	0.97	5.9	43	1.4
		d	D	1500-2100	4000	0.95	5.9	43	1.6
		e	D	2100-2700	3900	0.88	5.5	40	1.7
6	0.2	a	R	0-300	1300	1.15	1.9	29	1.1
		b	R	300-600	3500	1.28	5.5	52	0.9
		c	M	600-900	4900	1.29	7.9	60	1.2
		d	D	900-1200	4800	1.21	7.3	51	1.1
		e	D	1200-1500	5900	1.00	7.7	51	1.8
		f	D	1500-1800	5900	0.89	7.3	47	2.3
8	0.7	a	M	0-1000	11000	1.50	75	84	1.1
		b	D	1000-2000	7500	1.29	44	71	1.2
		c	D	5700-7400	4200	1.14	13	49	1.0
		d	D	7400-9100	2900	1.14	8.9	44	1.2
		e	D	17400-20800	400	1.06	0.53	11	0.6
4b <sup>d</sup>	0.3	a	R	0-500	800	1.1	1.5	23	1.7
		b	R+M	500-1000	3000	1.0	5.3	42	1.1
		c	M+D	1000-1500	4100	0.89	6.8	43	2.9
		d	D	1500-2100	5400	0.84	7.5	46	2.6
		e	D	2100-2700	4100	0.78	5.5	41	2.8

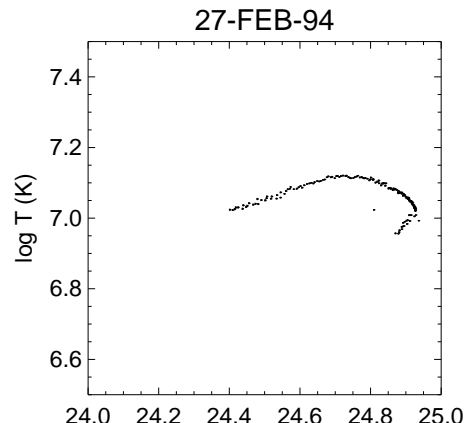
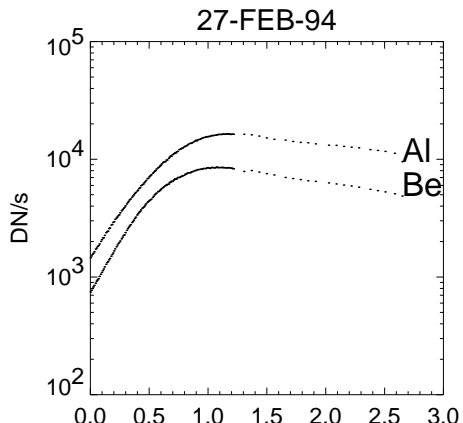
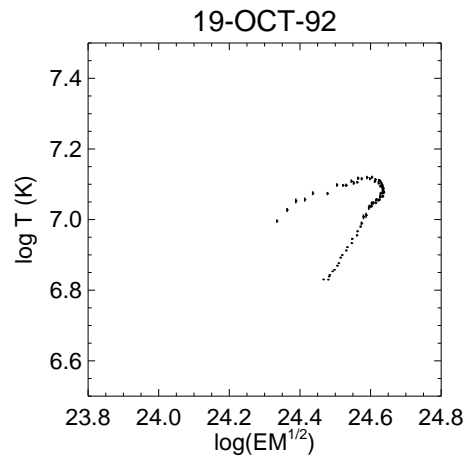
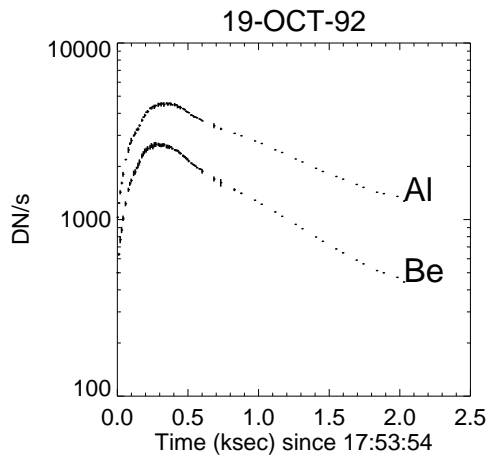
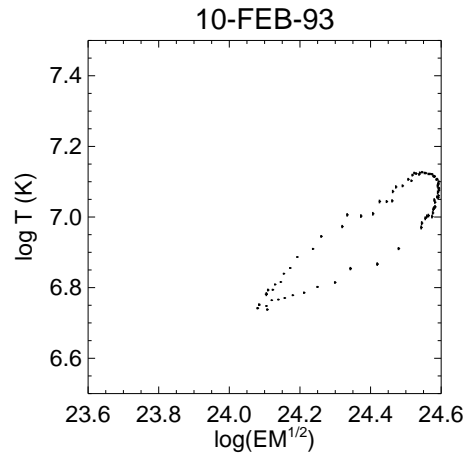
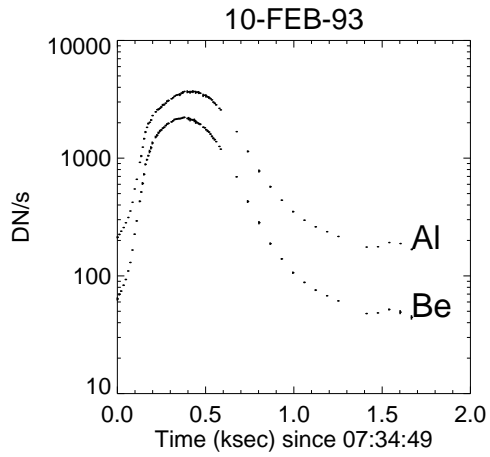
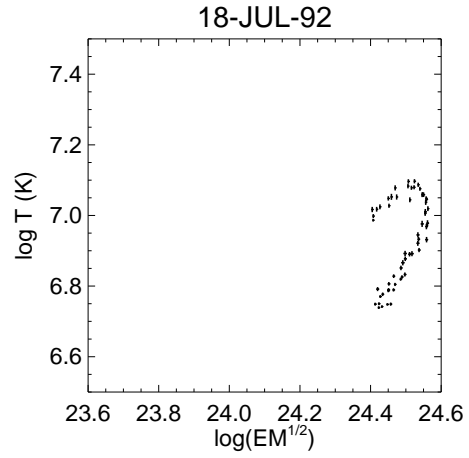
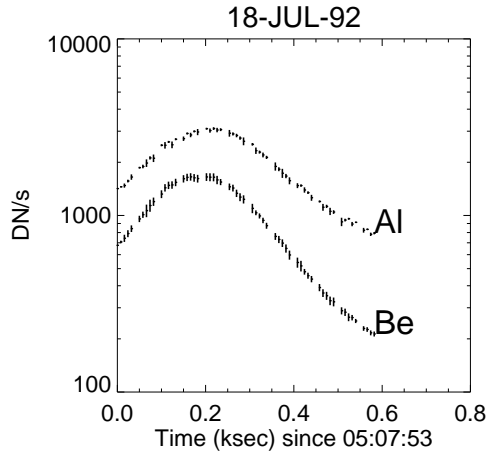
a - Distance at which the solar flare would yield the counts listed in the 6<sup>th</sup> column

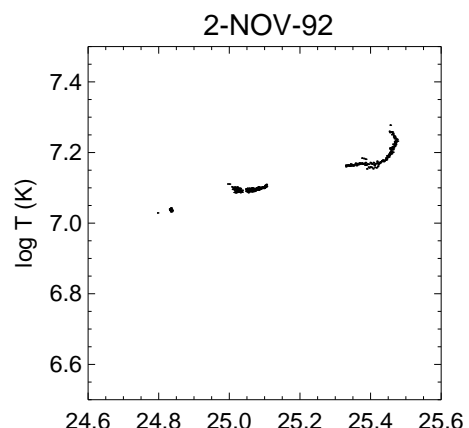
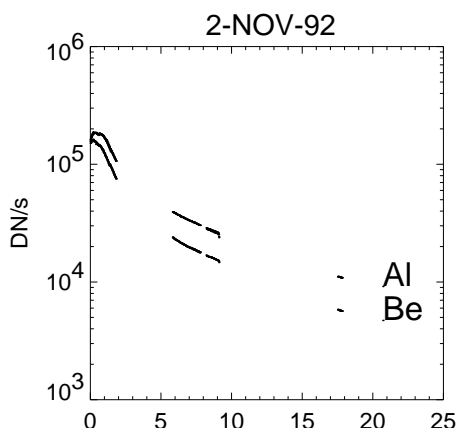
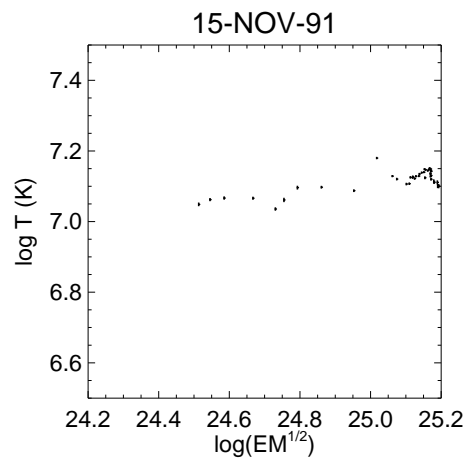
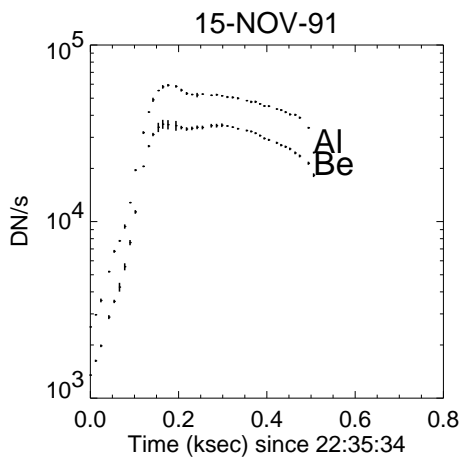
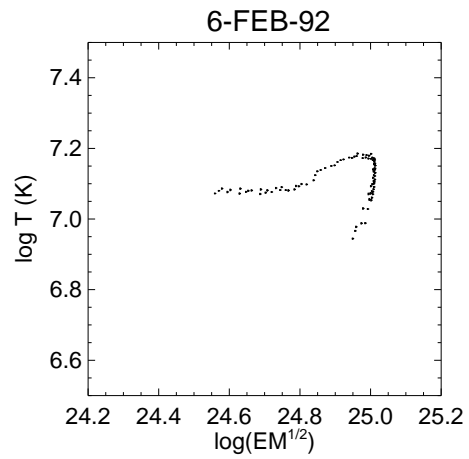
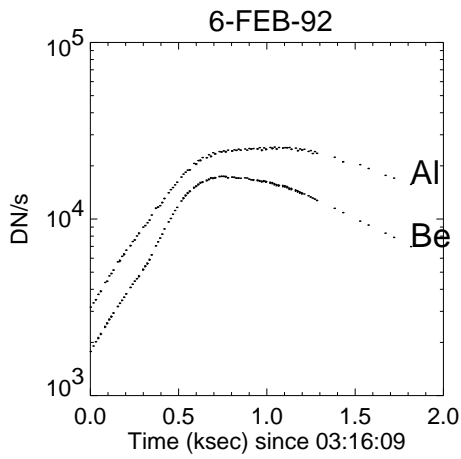
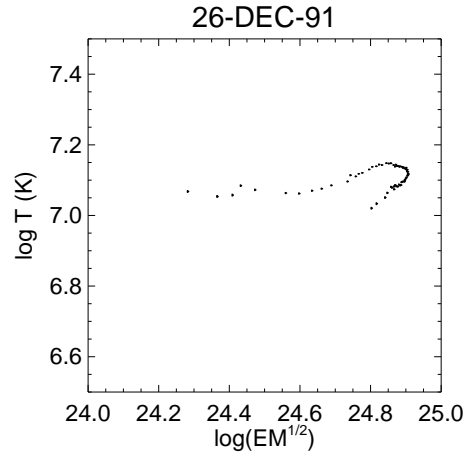
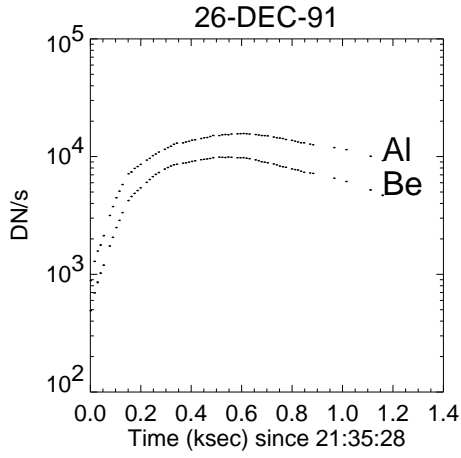
b - R = rising phase; M = around flare maximum; D = decay phase.

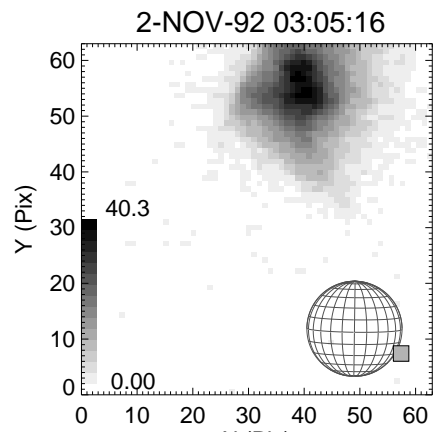
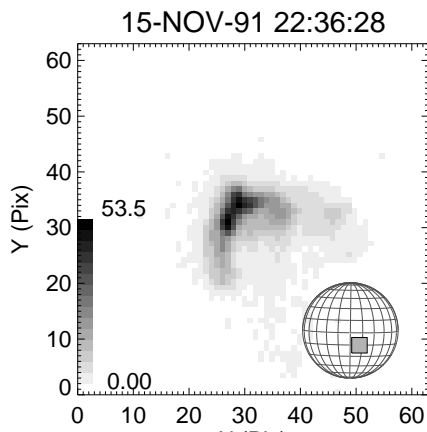
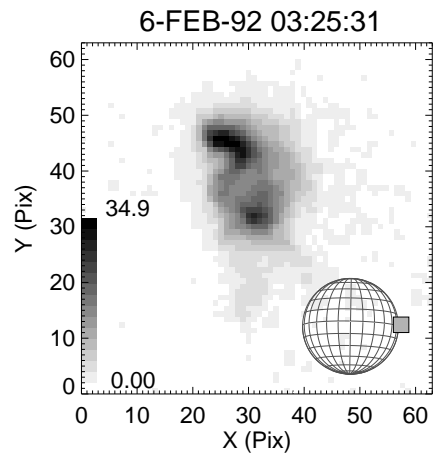
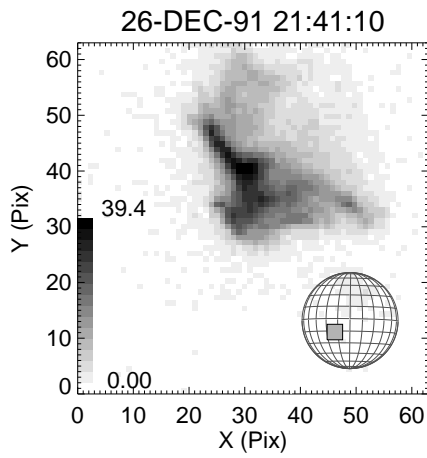
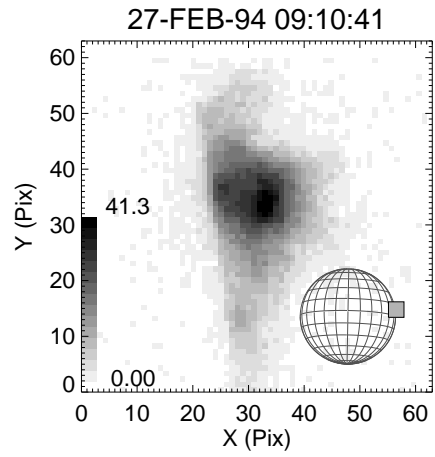
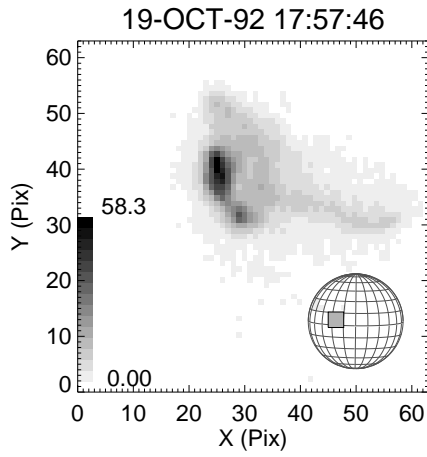
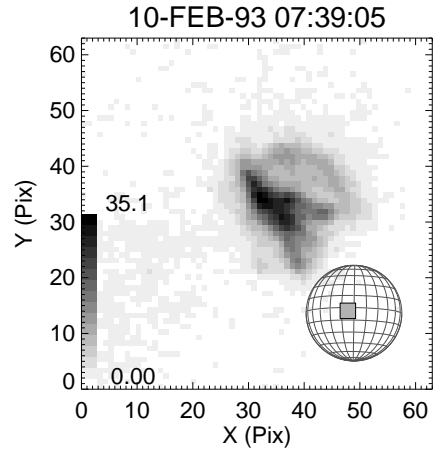
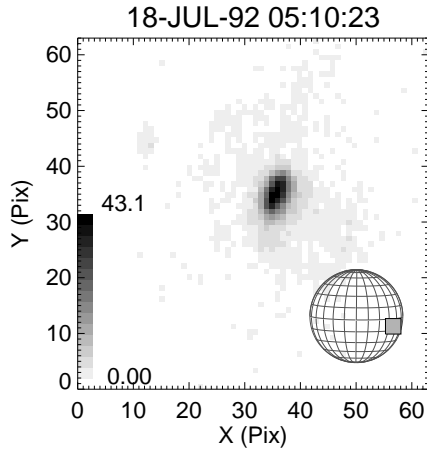
c - Reckoned since the beginning of the Yohkoh/SXT observation.

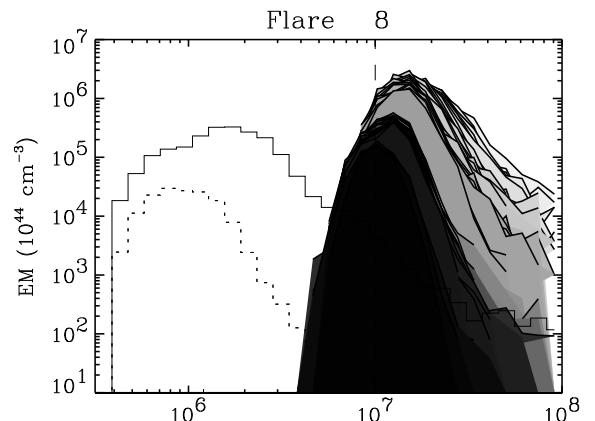
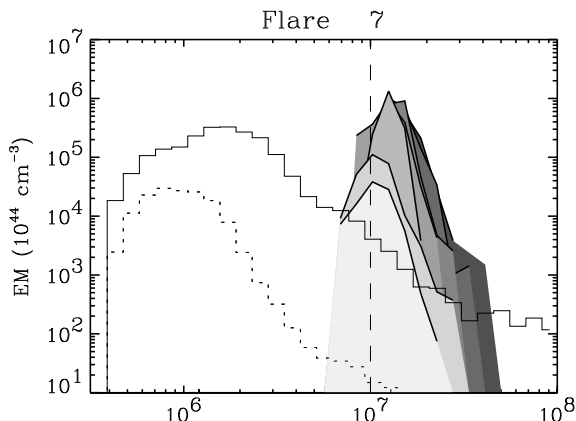
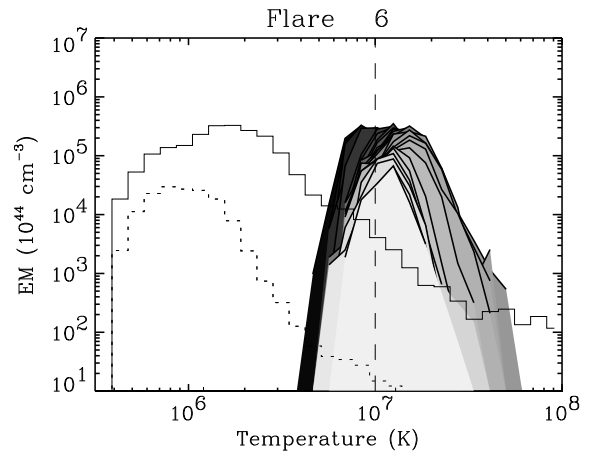
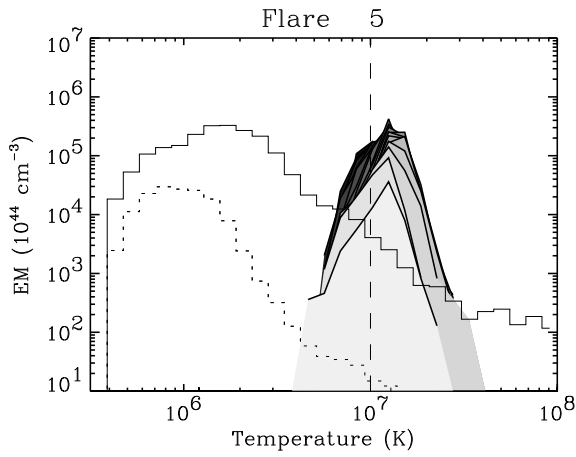
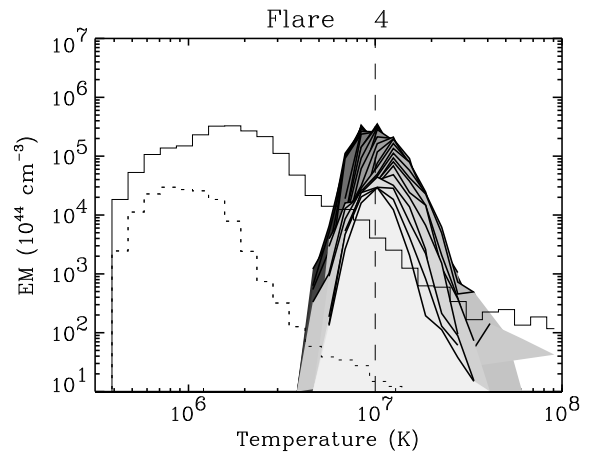
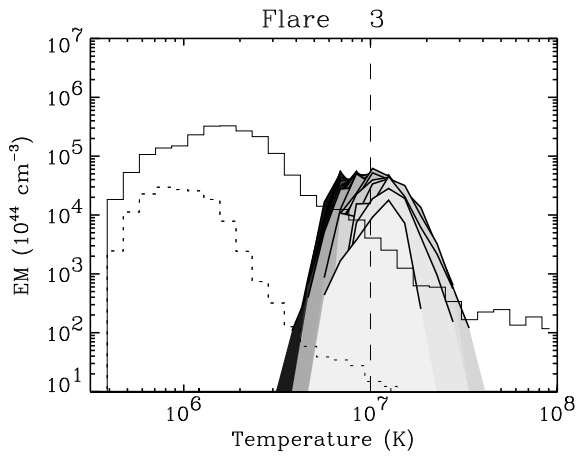
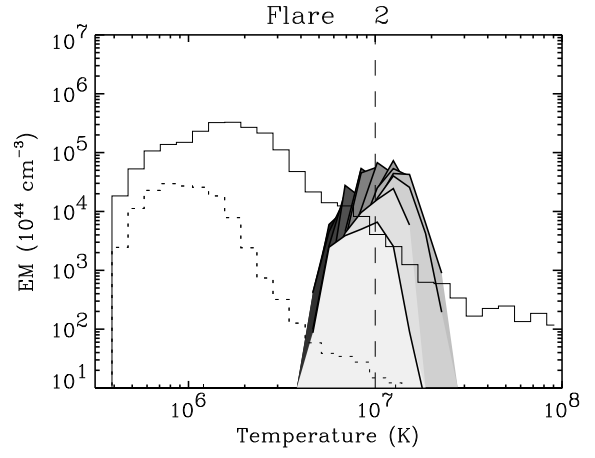
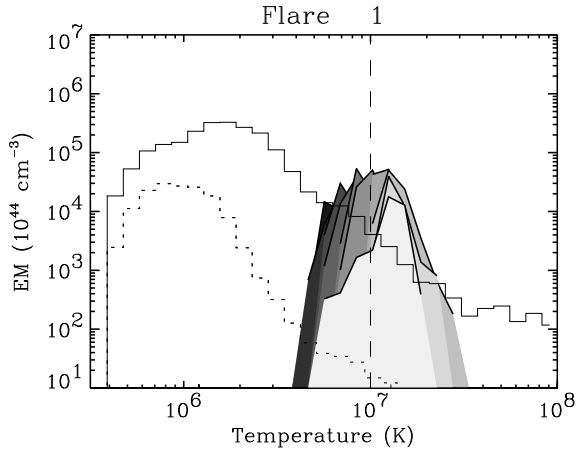
d - Spectra including contributions from the Yohkoh/SXT softer filter bands.











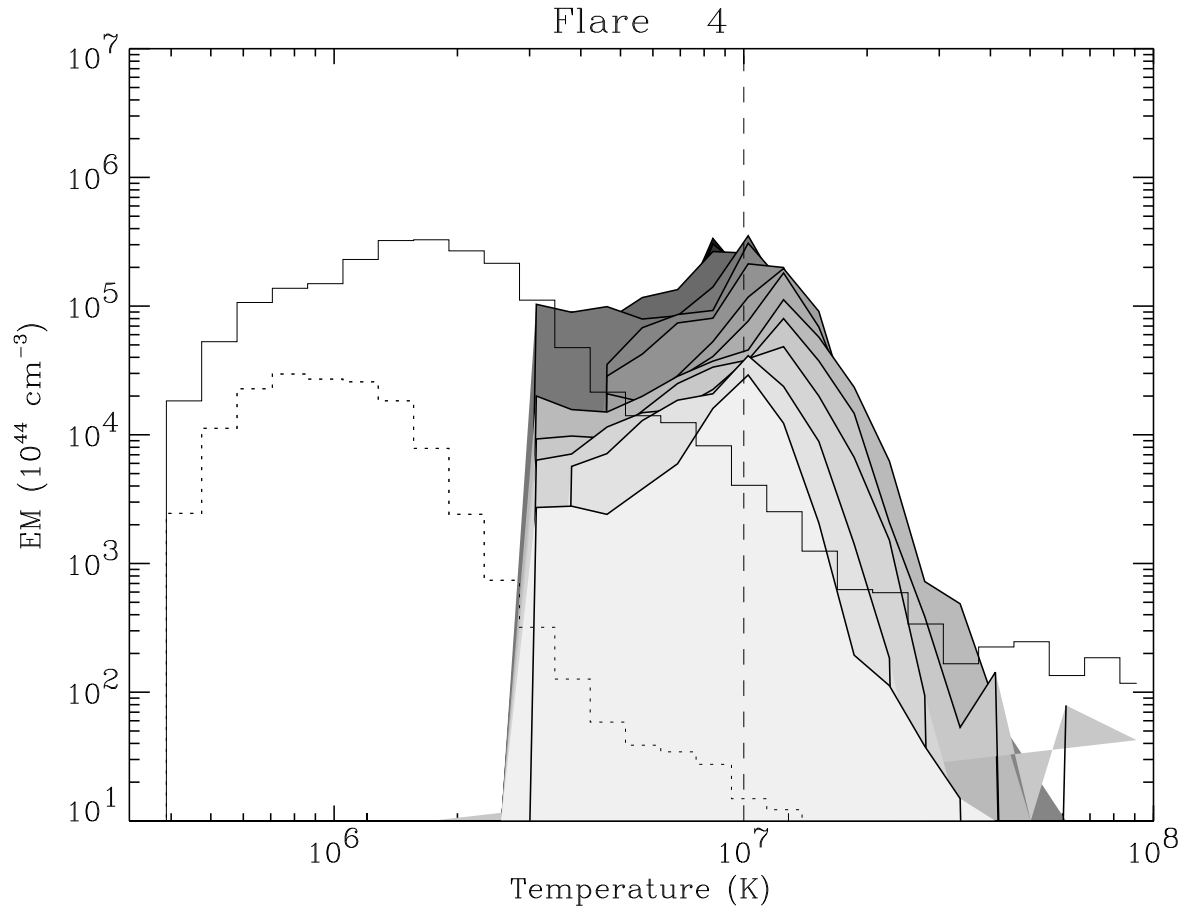


Fig. 5.—

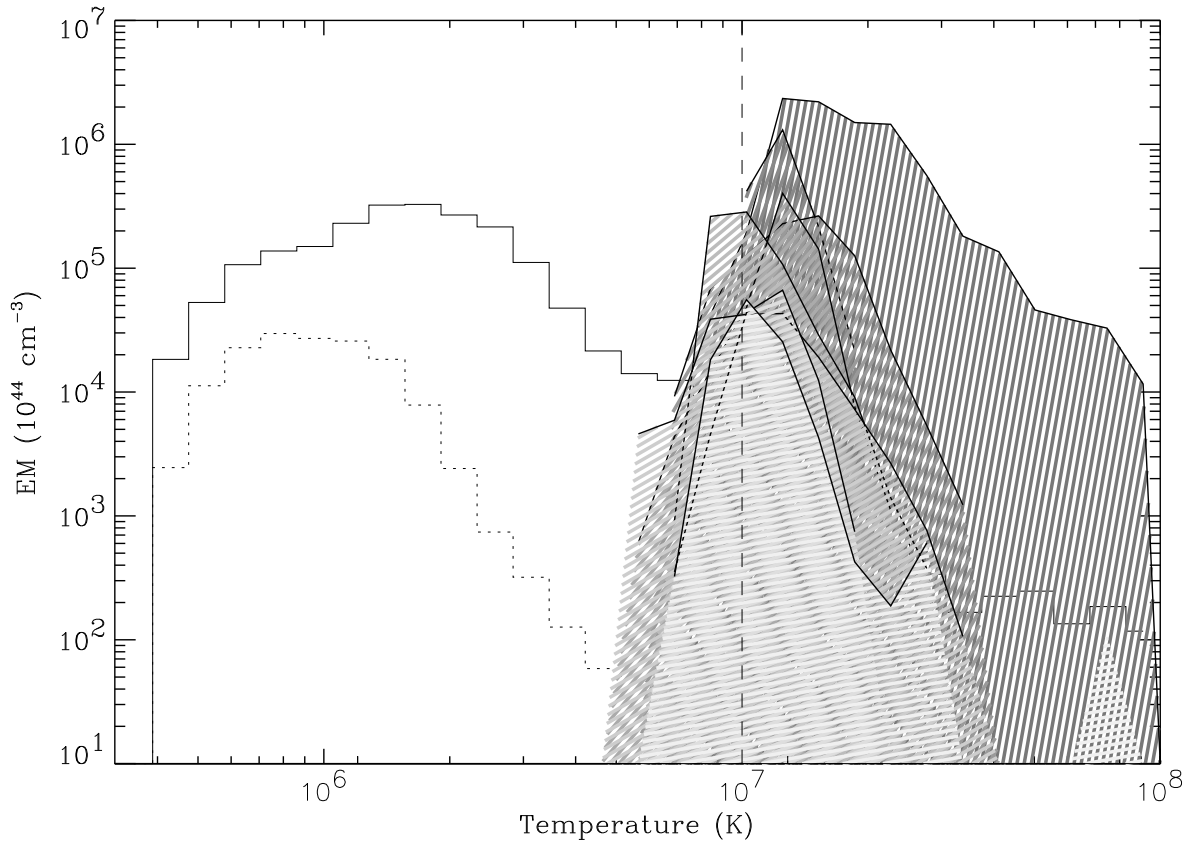


Fig. 6.—

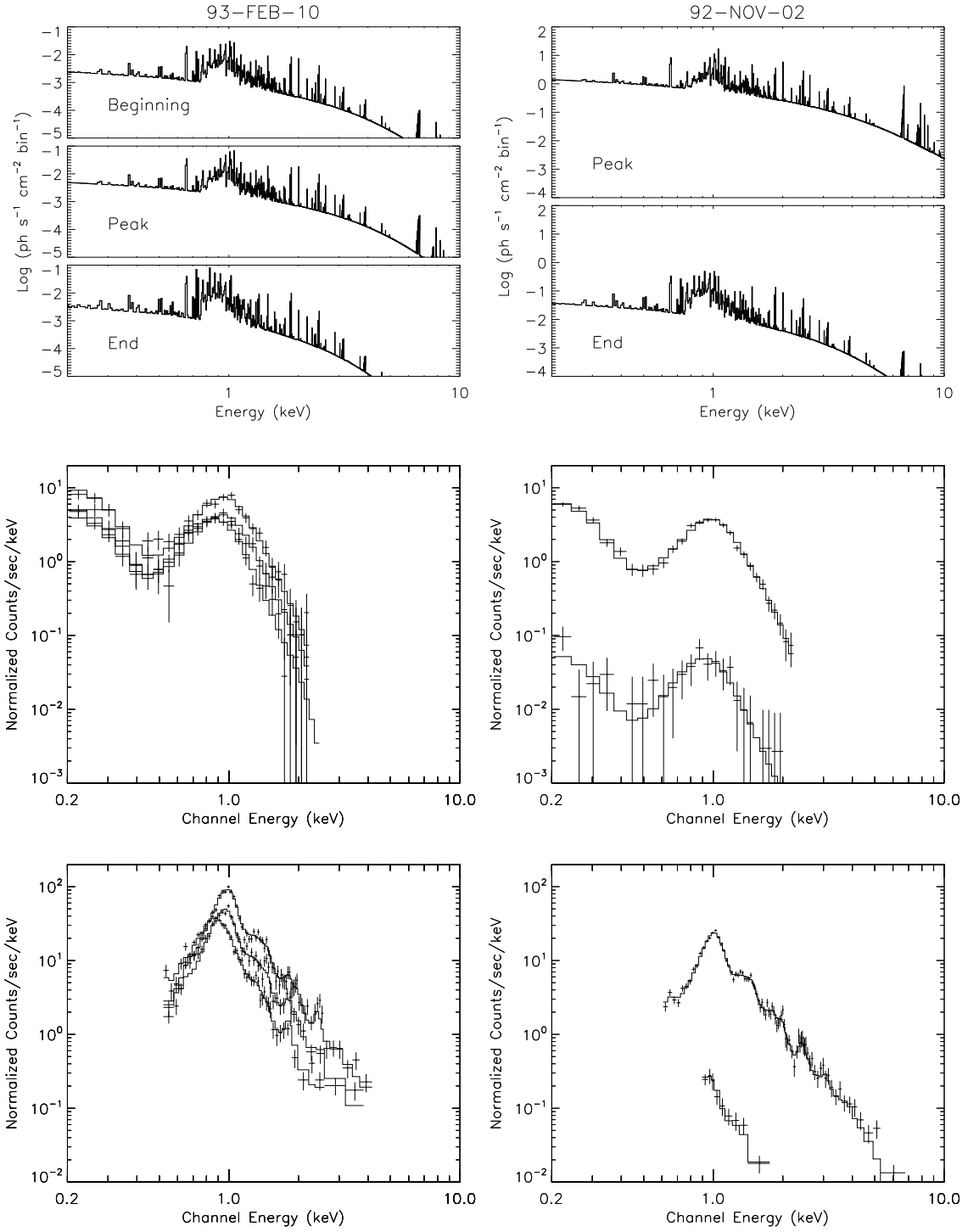


Fig. 7

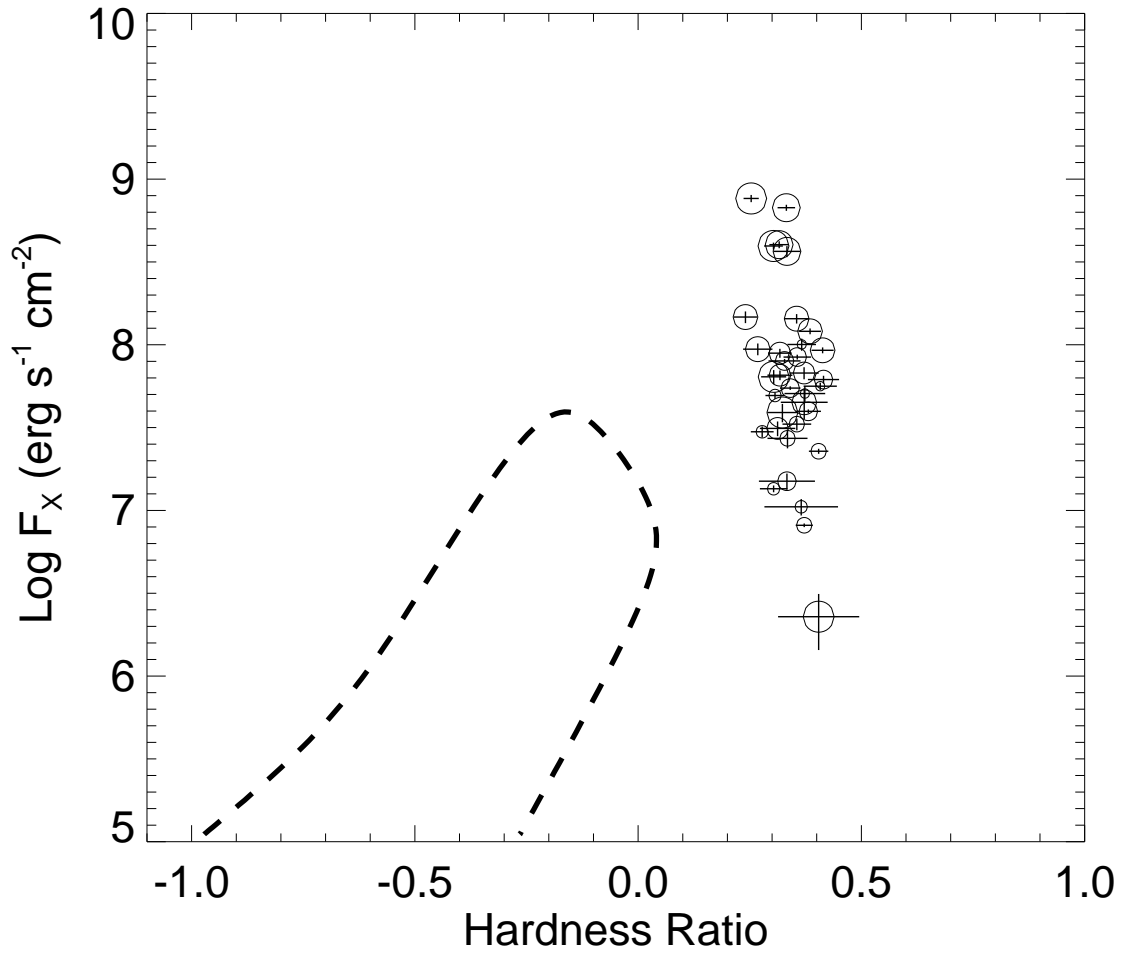


Fig. 8.—